Projecting impacts of climate change on metal mobilization at contaminated sites: Controls by the groundwater level

Jerker Jarsjö [a,*], Yvonne Andersson-Sköld [b,c], Mats Fröberg [d], Jan Pietroń [a], Robin Borgström [e], Åsa Löv [f], Dan B. Kleja [d,f]

[a] Department of Physical Geography, Bolin Centre for Climate Research, Stockholm University, SE-106 91 Stockholm, Sweden
[b] Environmental Department, Swedish National Road and Transport Research Institute (VTI), Box 8072, SE-402 78 Gothenburg, Sweden
[c] Architecture and Civil Engineering, Chalmers University, SE-412 96 Gothenburg, Sweden
[d] Swedish Geotechnical Institute (SGI), SE-581 93 Linköping, Sweden
[e] Ramböll Sverige AB, SE-211 11 Malmö, Sweden
[f] Department of Soil and Environment, Swedish University of Agricultural Sciences, Box 7014, Uppsala, Sweden

HIGHLIGHTS

- We model metal mobilization in response to climate-driven shifts in groundwater level
- Shifts in average level and fluctuation amplitude control mobilization from topsoil
- Topsoil heterogeneity in hydraulics and geochemistry explain change magnitudes
- A groundwater level increase of only 0.2 m can enhance mobilization by 200–1000%.

GRAPHICAL ABSTRACT
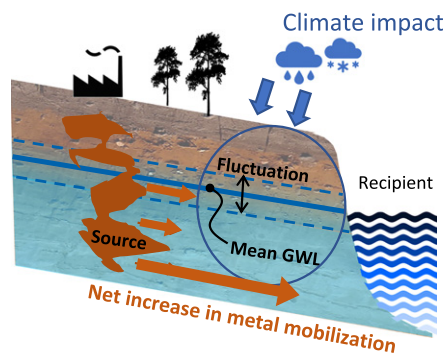
ARTICLE INFO

ABSTRACT

Heavy metal and metalloid contamination of topsoils from atmospheric deposition and release from landfills, agriculture, and industries is a widespread problem that is estimated to affect >50% of the EU's land surface. Influx of contaminants from soil to groundwater and their further downstream spread and impact on drinking water quality constitute a main exposure risk to humans. There is increasing concern that the present contaminant loading of groundwater and surface water systems may be altered, and potentially aggravated, by ongoing climate change, through large-scale impacts on recharge and groundwater levels. We investigated this issue by performing hydrogeological-geochemical model projections of changes in metal(loid) (As and Pb) mobilization in response to possible (climate-driven) future shifts in groundwater level and fluctuation amplitudes. We used observed initial conditions and boundary conditions for contaminated soils in the temperate climate zone. The results showed that relatively modest increases (0.2 m) in average levels of shallow groundwater systems, which may occur in Northern Europe within the coming two decades, can increase mass flows of metals through groundwater by a factor of 2–10. There is a similar risk of increased metal mobilization in regions subject to increased (seasonal or event-scale) amplitude of groundwater levels fluctuations. Neglecting groundwater level dynamics in predictive models can thus lead to considerable and systematic underestimation of metal mobilization and future changes. More generally, our results suggest that the key to quantifying impacts of climate change

---

* Corresponding author.
  E-mail address: jerker.jarsjo@natgeo.su.se (J. Jarsjö).

on metal mobilization is to understand how the contact between groundwater and the highly water-conducting and geochemically heterogeneous topsoil layers will change in the future.

1. Introduction

Contaminated soil is a recognized problem worldwide. For example, in Europe alone, >340,000 sites have been identified as contaminated according to data collection criteria of the 2011 European Environment Information and Observation Network (EIONET), comprising 11 EU member states (van Liedekerke et al., 2014). For an additional 2.5 million sites, unacceptable soil contamination is suspected, but not yet verified. The impact was recently emphasized in an assessment of soil heavy metals using the LUCAS topsoil database of almost 22,000 samples, which spatially cover all EU member states with a density of 1 sampling point per 200 km^2. The assessment showed that more than in 50% of samples, one or more heavy metals exceeded mean threshold levels used in Finnish legislation, which approximately reflects an average of the value range adopted by EU member states (Tóth et al., 2016).

Main sources of soil contamination by heavy metals and metalloids include atmospheric deposition of traffic emissions and other exhaust emissions, release from landfills, agriculture, mining, and other industrial activities, and accidental spills from transport and handling of various substances (Scott et al., 2005; Barth et al., 2009; Jarsjö et al., 2017a; Tóth et al., 2016). The typical outcome in all these cases is a vertical concentration gradient of metals in soil, with the highest concentrations in the topsoil. In addition to direct contact with contaminated soil, humans may be exposed via metal uptake in crops and edible plants (Nagajyoti et al., 2010; Raguž et al., 2013) or via water-borne spreading through e.g., coupled groundwater-surface water systems impacting drinking water wells (Mulligan et al., 2001; Hashim et al., 2011; Törnqvist et al., 2011).

Since previous industrial activities and current population densities are generally high near rivers and in coastal areas, many contaminated sites are located adjacent to water courses (e.g., Andersson-Sköld et al., 2007), which profoundly increases both the contamination risks and exposure risks (Destouni et al., 2010; Persson et al., 2011; Andersson et al., 2014). In addition, severe impacts of toxic long-lived substances such as heavy metals have been observed in coastal zones and at river mouths (Newton et al., 2012), where heavy metals may accumulate in sediments (e.g., Abrahim and Parker, 2008; Jaishankar et al., 2014; Naser, 2013; Pietroń et al., 2018). To reduce exposure risks, the influx of contaminants from soil to groundwater and their further downstream spread need to be reduced. Therefore, there is a critical need to identify and assess the sources and develop holistic and comprehensive regional and national abatement strategies (Schiedek et al., 2007; Naser, 2013; Karthe et al., 2017; Thorslund et al., 2017).

However, there is increasing concern that the present contaminant loading of groundwater and the subsequent transport to drinking water wells and surface waters, and the associated risks, may be altered, and potentially severely aggravated, by ongoing hydroclimatic change (Schiedek et al., 2007; Brandon, 2013; Colombani et al., 2016; Jarsjö et al., 2017b; Wijngaard et al., 2017). The global surface temperature increase by the end of this century is projected to be between 2 °C (based on the 2015 United Nations Climate Change Conference, COP 21 or CMP 11, Paris agreement) and 4 °C (if no strong measures are taken to reduce greenhouse gas emissions) (Barros et al., 2014; IPCC, 2014). This will impact the physical and geochemical properties of the soil-contaminant-groundwater system (e.g., Augustsson et al., 2011) and change the ice and snow patterns in high-latitude regions. Mean annual precipitation is also projected to increase in many temperate regions and the Arctic, including northern Europe and North America (Olsson

and Foster, 2014). Moreover, the frequency and intensity of rainfall events are likely to change, which may impact groundwater recharge patterns (Eckhardt and Ulbrich, 2003; Jyrkama and Sykes, 2007) and associated contaminant leaching and waterborne transport (Barth et al., 2009; Bonten et al., 2012). This is in addition to the impacts of climate-driven changes in frequency of catastrophic events, such as landslides, involving contaminated soil (e.g., Ströberg et al., 2017) or bark beetle outbreaks involving forest die-off and substance mobilization (e.g., Su et al., 2017).

Many of these climate-related changes will alter groundwater levels and groundwater flows, both annually and seasonally (Rodhe et al., 2009; Sundén et al., 2010; Vikberg et al., 2015). For instance, warmer winters in cold, snow-dominated regions will mean longer periods with unfrozen ground, earlier snowmelt, and precipitation in the form of rain instead of snow, which will increase groundwater recharge and, in turn, the average groundwater level (Eckhardt and Ulbrich, 2003; Sutinen et al., 2007; Okkonen and Kløve, 2011). This is consistent with predictions by Jyrkama and Sykes (2007) and Vikberg et al. (2015) that groundwater recharge and annual average groundwater levels in Sweden and Canada will, if anything, increase in the future as a result of climate change. On the other hand, in a warmer climate with higher evapotranspiration, spring and summer recharge and groundwater levels may be reduced (Eckhardt and Ulbrich, 2003; Okkonen and Kløve, 2011), which would mean increased seasonal variation (fluctuations) in groundwater levels.

On the time scale of hydrological events, shifting groundwater levels near streams can largely explain temporal changes in stream water quality (e.g., Seibert et al., 2009). In particular, when groundwater levels are high during hydrological events, there is preferential release of substances in parts of the topsoil temporarily influenced by the elevated groundwater level. This applies, for instance, for diffuse leaching of iron and carbon from topsoils, but may also apply for major and trace elements (Eklöf et al., 2015; Lidman et al., 2017). Based on three years of high-resolution measurements, Musolff et al. (2016) concluded that catchment-scale export of nitrate from a lowland agricultural region in Germany could be accurately predicted based on groundwater level data only.

However, several open questions remain regarding the extent to which climate-driven shifts in groundwater levels could lead to large-scale net changes in metal mobilization from contaminated topsoils. For instance, the patchy nature and complex hydrogeochemistry of metal-contaminated topsoils make large-scale systematic observations of their net loads quite challenging (Schiedek et al., 2007; Augustsson et al., 2011). To increase current understanding and aid future investigations, there appears to be a need for systematic model quantifications of potential impacts of shifting groundwater levels on such metal loads, which consider observed ('realistic') initial conditions and boundary conditions for contaminated sites subject to hydroclimate change.

In this study, we used 40-year series of groundwater level measurements, representing discharge areas in typical Northern European catchments with till soil, together with typical geochemical partitioning data for arsenic (As) and lead (Pb), in numerical modeling of future scenarios, in order to:

- determine the extent to which conceivable climate-driven changes in groundwater levels and fluctuation amplitudes can impact release of heavy metals (Pb and As) from contaminated topsoil
- identify factors leading to high climate sensitivity of metal release into groundwater (e.g., hydrogeological conditions, including

shallow-depth increases in hydraulic conductivity and heterogeneity in geochemical properties of topsoils).

2. Methods

2.1. Modeling approach

We focused our analysis on the upper parts of the soil profile, since anthropogenic pollution sources are generally more prevalent in topsoil than in deeper aquifer layers (e.g., Bonten et al., 2012). We considered pollution sources located in relatively low-lying groundwater discharge areas near or within the riparian zones of streams. Such sources have relatively high impacts on stream water quality, as mentioned above. In discharge areas, the depth to the groundwater is usually shallow. In addition, regional flow of groundwater, imported from higher parts of the catchment, usually dominates over local, vertical fluxes from infiltration of precipitation surpluses. The latter may be governed by quite different processes than the regional, near-horizontal groundwater flows considered here. Therefore these flow components need to be assessed using quite different approaches. The main focus in this study was on the contributions from the volumetrically dominating horizontal groundwater flow component.

We considered a model domain where metal(loid)s were partitioned into groundwater from a 'source zone' of contaminated topsoil, with subsequent metal(loid) release from this area with the flowing groundwater. From an environmental-societal perspective, surface water bodies (streams, rivers, wetlands and lakes), together with aquifers used for water supply, constitute recipients that should be protected from such groundwater-borne contaminants. Since potential natural attenuation of metal(oids) downstream of the source zone should not be relied upon (e.g., in environmental impact assessments) unless there is very thorough site-specific evidence of on-going and irreversible retention processes, the focus here was on the source zone release. The scenario analyses performed covered climate-induced effects of increased GWL and increased and decreased groundwater fluctuations on release of metal(loid)s from the source zone. The input data to the model were taken from an analysis of long-term monitoring data of groundwater levels made by the Geological Survey of Sweden (Sveriges Geologiska Undersökning; SGU, 2017). Lead and arsenic were chosen as model contaminants because their mobility is very different (see Section 2.6).

The model domain was configured to exemplify hydrogeological and geochemical conditions found for forested till soils in Northern Europe and North America. Such soils normally have gradients in hydraulic conductivity, which is highest close to the surface. Many man-made soil constructions, including various filling materials, also have high hydraulic conductivity in the upper part of the profile, as a result of use of sand-gravel fractions close to the ground surface (Löv et al., 2018).

2.2. Analysis tools and the modeling domain

A two-dimensional groundwater and solute transport model (Modflow NWT and MT3DMS using GMS 10.3.4), honoring Darcy's law and the continuity equation, was used to examine metal(loid) release and groundwater transport in our model domain. The total length of the modeled aquifer was 80 m (Fig. 1), and the depth of the active part of the model domain was 3.5 m. The model properties perpendicular to the slope and flow direction were assumed to be constant. Therefore, the results are scalable per unit width, which was arbitrarily set to 0.1 m. To account for the assumed importance of varying matrix properties with depth, the soil was divided into eight horizontal layers, which were assigned different values of hydraulic conductivity and different geochemical properties (Section 2.3).
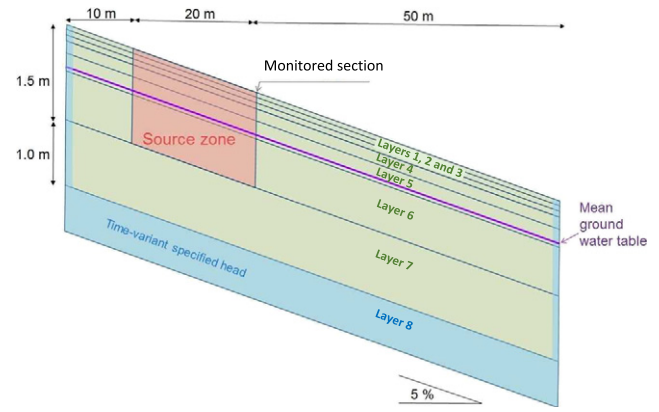

Fig. 1. Model set-up of the contaminated site, including the monitored section where the water flux and contaminant flows were monitored through the simulation.

Each of the layers consisted of 111 modeling cells, of width varying between 0.1 and 1 m. The ground surface was assigned a constant slope of 5% and the soil a constant porosity of 30%. The metal-contaminated area was represented with a uniform concentration of selected metal(loid)s in the top 1.5 m (layers 1–6) in a 20 m long zone, approximately 10 m from the upper boundary of the model (red area in Fig. 1).

The input water fluxes to the model are driven by groundwater fluctuations applied as a time-variant specified head at the upper (left) and lower (right) boundaries and at the bottom layer (layer 8). The base scenario was chosen to reflect field-observed groundwater level fluctuations on a daily time scale from a 41-year observational series, as described below.

The main output of the model consisted of time-series of metal concentrations C_L and groundwater flows Q_L in all eight layers (L) at a vertical, monitored section (Fig. 1), from which the total metal mass load M at time t was estimated as:

$$M(t) = \sum_L C_L(t) \cdot Q_L(t)/R \tag{1}$$

where R is a contaminant-specific retardation factor that can be related to the contaminant's partition coefficient (K_d, m³ kg⁻¹) as $R = 1 + K_d$ (ρ/n) in linear isotherm sorption models, where ρ is the soil bulk density (kg m⁻³) and n is the soil porosity [−]. The monitored section is located just downstream of the source and reflects the net contaminant loads released into the coupled groundwater-surface water system from the contaminated source.

2.3. Geochemical characteristics of the soil profile

To study metal(loid) mobilization at contaminated sites, Pb and As were used as model metal(loid)s. Contamination sources for Pb are e.g., mining activities, shooting ranges, glassworks, and oil residuals, while As contamination may originate from the use of wood preservatives, pesticides, and additives in alloys and glass raw materials (Swedish EPA, 2017). Lead and As can be considered two 'extremes' regarding contaminant mobility in soils and groundwater systems, where As is the more mobile of the two. However, enhanced transport of Pb by binding to particles, colloids, and dissolved organic ligands can be substantial in the upper part of the soil profile (Pédrot et al., 2008; Löv et al., 2018). For As, redox is a key variable, because the reduced form, arsenite (As(III)), is generally sorbed less strongly than the oxidized form, arsenate (As(V)) (Wilkie and Hering, 1996; Smedley and Kinniburgh, 2002). Thus, a low redox potential will favor mobilization of As.

The soil chemical data and contaminant concentration data were taken from a former wood impregnation site at Åsbro, central Sweden

(green star in Fig. 2), which is a particularly well-investigated site among >25,000 contaminated sites in Sweden (Swedish EPA, 2017). The total concentration of Pb and As in the topsoil (0–0.3 m) is 780 mg/kg and 2300 mg/kg, respectively. To account for the differing mobility of Pb and As, the contaminant transport modeling routine considered a linear isotherm, i.e., a partition coefficient (K_d, m³ kg^{-1}), approach. The geochemical input data to the model were taken from an irrigation experiment conducted on intact soil profiles extracted from the topsoil (0–0.3 m) at the Åsbro site (Löv et al., 2018). Four replicated soil columns were subjected to an irrigation intensity of 2 mm h^{-1} for 10 days. The K_d values of Pb and As(V) used in simulations were obtained from total soil concentrations and time-integrated average leachate concentrations (4 sampling occasions), representing the average values of all four soil columns. The experiment was conducted under unsaturated conditions, but it was assumed in the present study that the concentrations in leachate were representative of those under saturated flow conditions, because equilibrium conditions were achieved and the contribution of preferential water flow was negligible during the experiment (Löv et al., 2018). For Pb, there was a major contribution of particulate transport in this soil (92%) (Löv et al., 2018). In the simulations, we assumed that particle-facilitated transport of Pb was possible in the upper 50 cm of the soil profile, giving 11-fold lower K_d values in layers 1–4 compared with layers 5 and 6 (Table 1). In this respect, Pb represents an element with higher mobility in the topsoil than in the subsoil. Since the irrigation experiment was run under

unsaturated flow conditions, i.e., oxic conditions, the As in leachate was mainly present as As(V). Accordingly, the K_d value of As (V) adopted in the simulations was based on the experimental data. In order to obtain a realistic K_d value for As(III), we assumed a value that was 23-fold lower than the measured value for As(V). Based on information obtained for ferrihydrite systems, this value seems to be reasonable (Wilkie and Hering, 1996), although the relative binding strength can vary substantially with e.g., presence of different types of iron (Fe) and aluminum (Al) (hydr)oxides, pH value, and solute-sorbent relationship (Smedley and Kinniburgh, 2002). As shown in Table 2, the K_d data on Pb and As(V) for Åsbro are quite similar to the median values found for a large number of contaminated sites in Sweden.

2.4. Hydraulic conductivity in the soil profile

Data on the relative change in saturated hydraulic conductivity K with soil depth were based on measurements at a number of sites (Boelter, 1968; Mehuys and De Kimpe, 1976; Lundin, 1982; McKay et al., 1993; Nyberg, 1995; Bergvall et al., 2011), the positions of which are indicated by pink diamonds in Fig. 2. The absolute (reference) hydraulic conductivity was taken from the Gårdsjön catchment in Sweden (pink star in Fig. 2). Northern forested glacial till soils are commonly characterized by significantly decreasing saturated hydraulic conductivity (K_S, m s^{-1}) with increasing depth according to a power law relationship (Lind and Lundin, 1990; Nyberg, 1995; Lundmark and
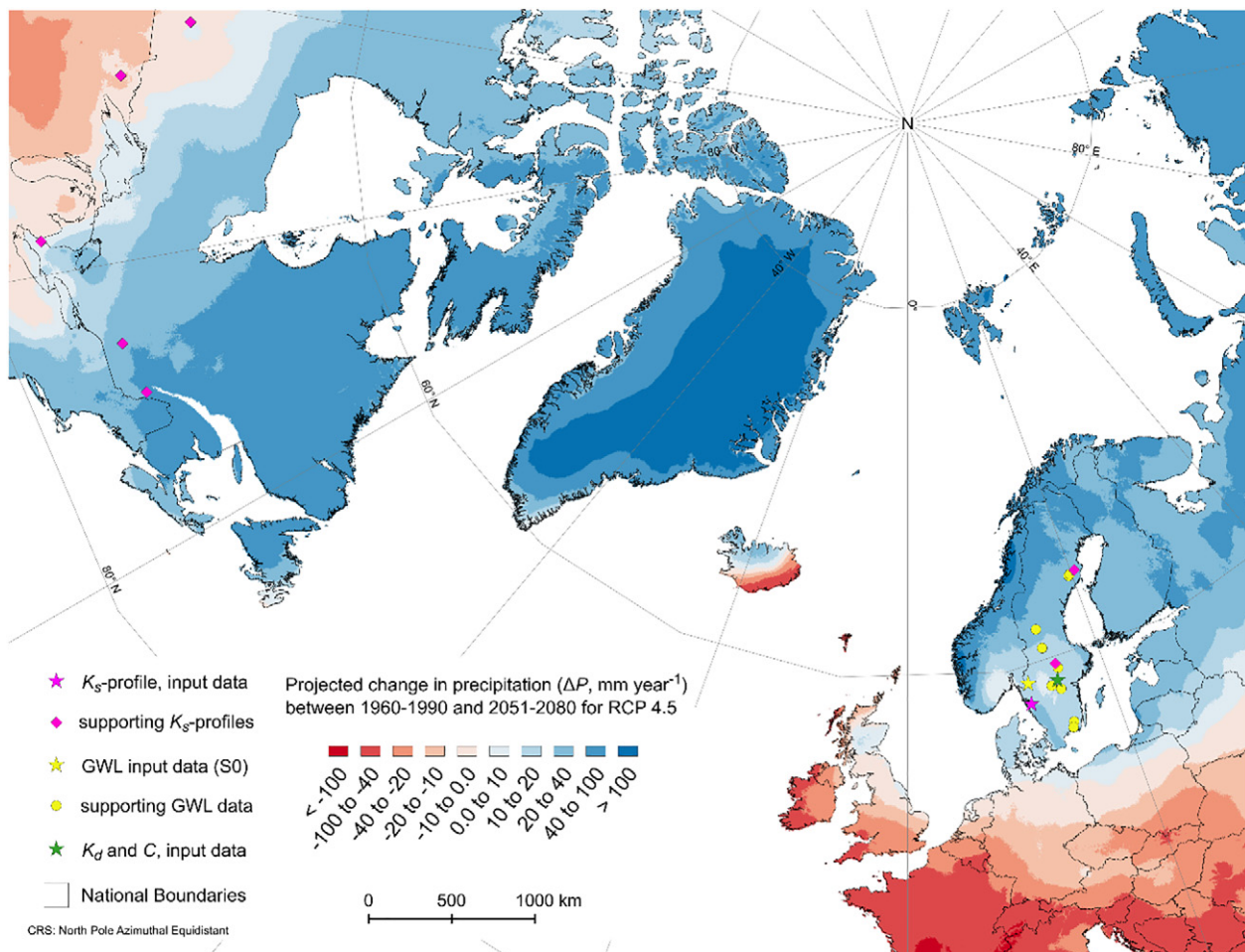

Fig. 2. Map showing sampling locations for geochemical and hydrological input datasets, including partition coefficient (K_d) and metal concentration (C) in soil at contaminated sites, hydraulic conductivity (K) (Boelter, 1968; Mehuys and De Kimpe, 1976; Lundin, 1982; McKay et al., 1993; Nyberg, 1995; Bergvall et al., 2011), and groundwater level (GWL) (SGU, 2017). The colors indicate projected future precipitation changes (multimodel ensemble mean of the Coupled Model Intercomparison Project, Phase 5 (CMIP5) output for IPCC's Representative Concentration Pathway (RCP) 4.5 trajectory; WorldClim, 2018) (increases in blue and decreases in red).

Table 1
Model input: Groundwater concentrations (C, g m^{-3}), of Pb, As(V), and As(III) within the contaminated area (red area in Fig. 1) and partition coefficient, K_d (m^3 kg^{-1}). Soil concentration was set at 780 mg/kg and 2300 mg/kg for Pb and As, respectively, in all modeling layers 1–8.

Layer	Depth, h (m)	Lead (Pb)		Arsenate (As(V))		Arsenite (As(III))	
		Concentration in water, C (g m^{-3})	Partition coefficient, K_d (m^3 kg^{-1})	Concentration in water, C (g m^{-3})	Partition coefficient, K_d (m^3 kg^{-1})	Concentration in water, C (g m^{-3})	Partition Coefficient, K_d (m^3 kg^{-1})
1	0.0–0.1	0.078	10	3.4	0.68	77	0.03
2	0.1–0.2	0.078	10	3.4	0.68	77	0.03
3	0.2–0.3	0.078	10	3.4	0.68	77	0.03
4	0.3–05	0.078	10	3.4	0.68	77	0.03
5	0.5–0.8	0.0071	110	3.4	0.68	77	0.03
6	0.8–1.5	0.0071	110	3.4	0.68	77	0.03
7	1.5–2.5	0	110	0	0.68	0	0.03
8	2.5–5.0	0	110	0	0.68	0	0.03

Jansson, 2009; Bishop et al., 2011). Following Bishop et al. (2011), we expressed this relationship as:

$$K_S(z) = K_S^* \cdot (z/z^*)^{-1.22} \tag{2}$$

where z (m) is the depth below the soil surface and K_S^* (m s^{-1}) is a reference hydraulic conductivity for a given reference depth z^* (m). We used $K_S^* = 9.0 \times 10^{-6}$ m s^{-1} for depth $z^* = 0.78$ m as reported by Nyberg (1995) for the Gårdsjön basin, which yielded an estimated K_S value ranging from about $2.6 \cdot 10^{-4}$ in model layer 1 to $2.9 \cdot 10^{-6}$ in model layer 7 (Fig. 3a).

2.5. Historical groundwater level dynamics (base scenario)

To represent the historical groundwater level dynamics, we screened the dataset of the Geological Survey of Sweden (SGU, 2017) for wells located in the so-called critical zone of groundwater-surface water exchanges that can have large impact on downstream conditions (e.g., Clark et al., 2015). The specific selection criteria were that the wells should have shallow average groundwater level (≤1 m from the ground surface) and be located in discharge areas 150 m or less from surface waters. In total, 10 wells spread across Sweden (Fig. 2; yellow symbols) matched these criteria (Table 3). For these 10 wells, the median of the long-term average depth from the ground surface to the groundwater level was 0.73 m, and the median of the standard deviation was 0.34 m (Table 3).

In our numerical modeling, such long-term historical conditions were considered in a base scenario (S0), taken as the full time series data of well 71_1, from 15 November 1976 to 31 October 2017 (black curves in Fig. 3b and c; Table 3). In this well, the groundwater level dynamics were most similar to the median of the 10 wells considered in

Table 2
Comparison of partition coefficient (K_d) values obtained for the Åsbro soil with results from a compilation by Fanger et al. (2006) for contaminated sites in Sweden. K_d-unfiltered values are based on total concentrations in soil leachate, K_d-filtered values on filtered (0.45 μm) solutions. Fanger et al. (2006) obtained their data in leaching tests using a leachate-to-solid ratio (L/S) of 2. The data for Åsbro were obtained in an irrigation experiment on intact soils (Löv et al., 2018). n = number of samples, sd = standard deviation.

Site/data	Lead (Pb)		Arsenic (As)	
	K_d-unfiltered (m^3 kg^{-1})	K_d-filtered (m^3 kg^{-1})	K_d-unfiltered (m^3 kg^{-1})	K_d-filtered (m^3 kg^{-1})
Åsbro	10	110	0.6	0.68
Mean[a]	–	370	–	8.8
Median[a]	–	36	–	0.89
n[a]	–	48	–	60
sd[a]	–	824	–	23

[a] Compilation by Fanger et al. (2006) of contaminted sites in Sweden

terms of both the long-term average groundwater level (0.75 m) and the fluctuations (standard deviation of 0.39 m).

2.6. Formulation of future scenarios for groundwater level dynamics

With climate change, some areas in the northern hemisphere are expected to experience higher groundwater levels, as summarized in the introduction to this paper. Fig. 2 shows areas where the average future precipitation in Northern Europe and North America is expected to increase (blue areas), potentially with average groundwater level increases as a result. In addition to a change in mean groundwater level, the amplitude of the groundwater fluctuations may decrease in some regions, e.g., since infiltration may become more uniform throughout the year as a result of shorter periods with ground frost. On the other hand, the amplitude of the groundwater fluctuations may increase if extreme precipitation or drought events become more common. Overall, it is highly uncertain whether, and to what extent, there will be such intra-annual (e.g., seasonal) shifts in mean groundwater level (e.g., Kløve et al., 2014; Vikberg et al., 2015). Because of these uncertainties, effects of increases and decreases in the amplitude of groundwater fluctuations were tested in this study, in addition to effects of increased mean groundwater level.

In our numerical modeling, we formulated and explored four different main scenarios (S1 to S4) of possible future, climate-driven changes from the historical conditions of the Base Scenario S0 (Section 2.5). The scenarios accounted for plausible groundwater level increases and changes in groundwater level fluctuations, as listed in Table 4 and illustrated in Fig. 4. In order to examine the impacts of neglecting groundwater level fluctuations in numerical simulations, we also formulated two hypothetical time-invariant scenarios where all groundwater level fluctuations were removed and the groundwater level was kept at a constant value (scenarios S0* and S1* in Table 4).

Regarding the magnitude of assumed groundwater level increase in the coming two decades, we departed from the historical compilation of Swedish groundwater wells within the critical groundwater-surface water interaction zone (Table 3), which showed an increasing groundwater level trend with time for most of the 10 wells, e.g., the level during the recent time period 2007–2016 was up to 0.21 m closer to the ground surface than in the time period 1987–1996 (Table 3). In our future scenarios S1, S3, and S4 (Table 4), we assumed a further mean increase in groundwater level of the same magnitude (0.2 m) during the coming two decades. In scenario S1 (blue curves in Fig. 3a and b), the input groundwater levels were simply obtained by adding a constant of 0.2 m to the readings in the base case scenario groundwater level series (S0; black curves in Fig. 3, obtained from well 71_1). In scenario S2 (green curves in Fig. 3), the average groundwater level was assumed to remain unchanged, but the amplitude of the base case (S0) groundwater level fluctuations was increased by multiplying all deviations from the mean by a factor of 1.5. By definition, this operation led to an increase in the standard deviation around the mean of 1.5 (Table 4).
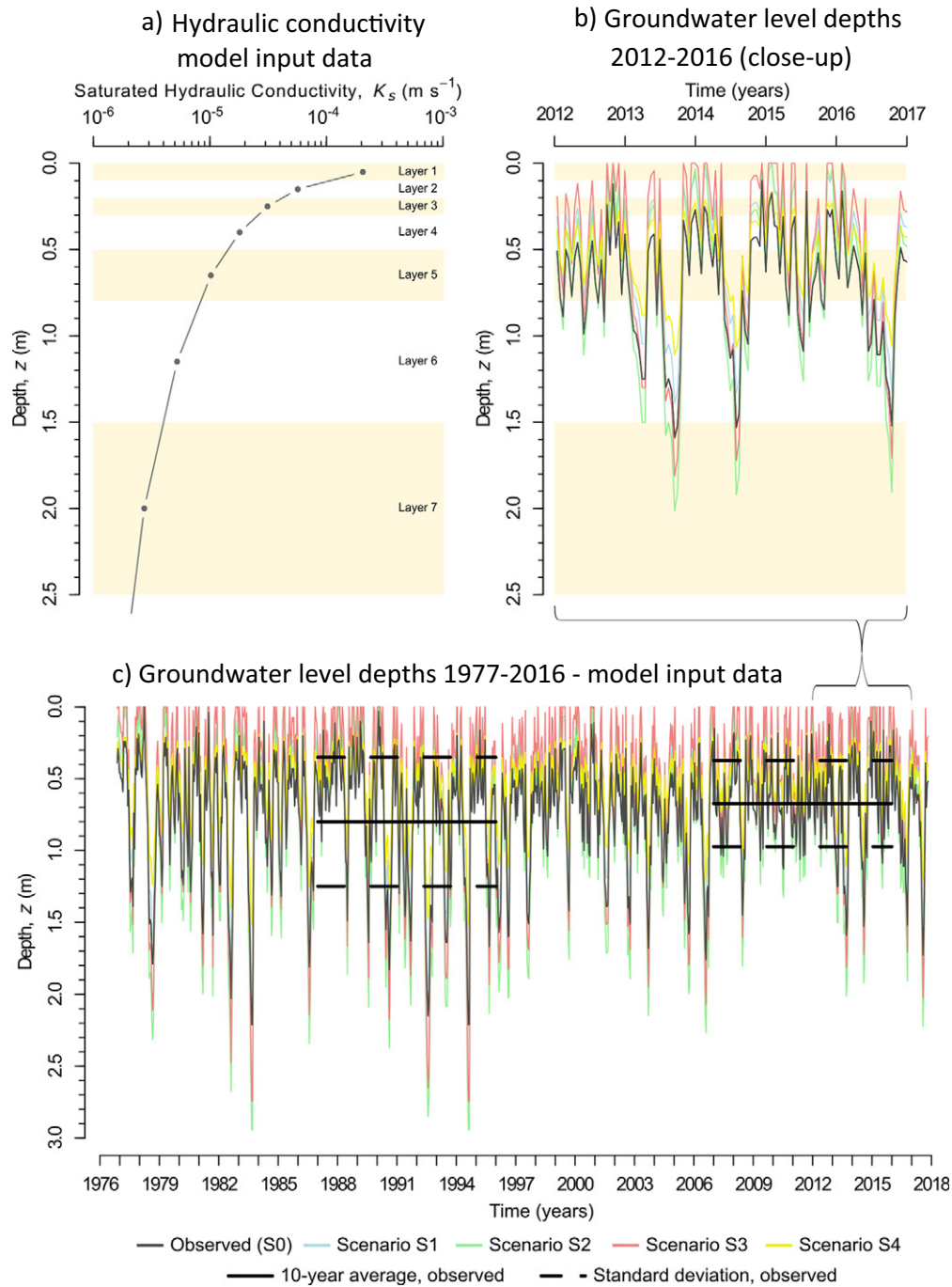
Fig. 3. Summary of hydrogeological input data to the model. (a) Estimated saturated hydraulic conductivity (K_S) for natural Northern European till soil applied in the modeled soil layers 1–7. (b) Five-year (2012–2016) close-up and (c) whole series of the groundwater level data used. Well 71_1 observations, which constitute the historical base scenario (Section 2.5), are shown in black and formulated future scenarios S1-S4 (see Section 2.6), obtained by displacing and/or stretching the well 71_1 data, are shown in different colors. The thick horizontal lines in (c) illustrate the changed mean groundwater level (black line) and standard deviation (dashed line) of the black curve (well 71_1 data) between the 10-year periods around 1990 and 2010.

For S3 (red curves in Fig. 3), the same amplifying multiplication using a factor of 1.5 was performed, however modifying the S1 data (green curve) representing elevated groundwater level, instead of the base case S0 data. In scenario S4 (yellow curves in Fig. 3), the amplitude of the S1 data was decreased by multiplying by a factor of 0.67. The resulting wide range of fluctuations considered in the future scenarios (S2, S3, and S4), from a decrease in standard deviation by a factor of 0.67 to an increase by a factor of 1.5 (Table 4 and Fig. 4), fully covered the smaller range of observed standard deviation difference ($\Delta\sigma$) in the 10 wells considered (Table 3).

3. Results

3.1. Current and projected future groundwater flows

The simulated groundwater flow through different topsoil layers (numbered according to Fig. 1) and the total groundwater flow are illustrated for different model scenarios (black and colored bars) in Fig. 5. In the base scenario S0 (black bars), representing observed historical groundwater levels, most of the total simulated groundwater flow occurred below 0.8 m depth, in layers 6 (39%) and 7 (34%). The total

Table 3
Summary of the data series from the considered wells.

SGU code[a] for well	Well coordinates		Measurement period	$\overline{GWL}$[b] (m)	$\Delta\,\overline{GWL}$[c] (m)	σ_{GWL}[d] (m)	$\Delta\sigma_{GWL}$[e] (m)	$\Delta\sigma_{GWL}$[e] (%)
	North	East						
71_1	**59.1723**	**12.1190**	**1977–2016**	**0.75**	**-0.12**	**0.39**	**−0.15**	**−32%**
5_4	56.6065	15.5500	1963–2014	0.59	0.23	0.46	−0.04	−8.9%
89_7	59.6227	15.4336	1985–2016	0.73	-0.10	0.18	−0.06	−29%
50_13	60.8802	14.3624	1974–2015	0.5	-0.08	0.15	−0.05	−38%
68_4	61.9375	14.2071	1977–2010	0.52	-0.01	0.27	−0.05	−17%
33_202	64.1866	19.5738	1983–2016	0.81	-0.21	0.49	−0.07	−14%
16_94	58.7839	14.3541	1983–2016	0.92	-0.01	0.35	−0.07	−18%
33_104	64.2551	19.7792	1983–2016	0.99	-0.21	0.26	−0.06	−24%
60_46	58.4967	15.1906	1975–2015	0.73	-0.08	0.63	−0.22	−29%
72_103	56.3146	15.3590	1974–2013	0.57	-0.07	0.33	−0.03	−8.8%
			Median:	0.73		0.34		

Bold: Well data used as base scenario.
[a] SGU (2017).
[b] Mean groundwater level (m below ground surface), 1987–2016.
[c] Difference in mean GWL (m below ground surface), 2007–2016 compared with 1987–1996.
[d] Fluctuation, expressed as standard deviation σ around the mean GWL, 1987–2016.
[e] Difference $\Delta\sigma$ in GWL fluctuation, 2007–2016 compared with 1987–1996.

flow was 13.4 m³ year⁻¹ m⁻¹ (Fig. 5). Under these historical conditions, the groundwater level repeatedly fell below 1 m depth (Fig. 3c). This reduced the amount of water passing through the top 0.8 m (layers 1–4) of the till soil profile, despite the fact that the topsoil (0–0.3 m) has higher hydraulic conductivity than the deeper layers (Fig. 3).

However, the relatively modest future increase in average groundwater level considered, of 0.20 m (from 0.75 m depth (base scenario S0; Fig. 5)) to 0.55 m depth (scenarios S1, S3, and S4; Fig. 5), meant that the top 0.30 m (layer 1–3) of the soil profile was much more active in conveying groundwater. A similar effect was observed on increasing the amplitude of groundwater level fluctuations while keeping the average groundwater level at 0.75 m (scenario S2; Fig. 5). In particular, the flow through the topsoil was estimated to increase by up to 60-fold in the top 0.30 m. In the whole soil domain considered, the net impact of increased groundwater level fluctuations around the average level was considerable (scenario S2; 26% higher total flow compared with S0), although somewhat smaller than the net impact of increased average groundwater level (scenario S1; 48% higher total flow). Hence, if both fluctuations and average levels increase in the future, the flow of the domain will increase considerably (scenario S3; 89% higher flow compared with S0). Notably, the combined impact of increased groundwater level and decreased fluctuation amplitude (S4) resulted in similar groundwater flow as in the scenario with just increasing amplitude (S2), although the contribution from the top 0.30 m in the former scenario (S4) was smaller (Fig. 5).

3.2. Current and projected future mass flows of As and Pb

The largest proportion of the annual average mass flows of As (V) and As(III) ($M_{As(V)}$ and $M_{As(III)}$, respectively) released from contaminated soil in the source zone (Fig. 1) during the 41-year historical simulation period 1977–2016 (scenario S0) occurred around and below 1 m depth from the soil surface, i.e., in layers 5 and 6 (Fig. 5). This is consistent with the fact that these layers convey a higher water flow, Q_L, than the surrounding domain (Section 3.1).

The total mass flow of As(V) and As(III) in all future scenarios S1 to S4 increased more than the accompanying increase in water flow (Section 3.1), in total by around 82% (scenario S1), 46% (scenario S2), 150% (scenario S3), and 44% (scenario S4), compared with the base scenario (S0). Furthermore, analogously to the pattern of flow increases, the highest mass flow increases compared with the historical simulation period (scenario S0) were seen in the top 30 cm of the soil profile for scenario S3, with 730% higher mass flow of As(III) and 1440% higher mass flow of As (V). A general trend for all scenarios S1 to S4 was that the upper part of the soil profile actively released and conveyed a considerable fraction of the total metal transport, whereas the contribution from the upper soil profile was negligible in the base scenario S0.

Interestingly, the absolute mass flow of As(III) was approximately 1000-fold higher than the mass flow of As(V) (Fig. 5), for the base scenario S0 and for the future scenarios S1-S4. Thus, the simulations illustrate the large effect of the lower binding strength of As(III) compared

Table 4
Scenario formulation summary, including base scenario S0 (historical conditions; see also Section 2.5 and Fig. 4), future scenarios S1–S4 (Section 2.6), and hypothetical time-invariant scenarios S0* and S1* (Section 2.6).

Scenario name and figure reference	Represented condition	Mean groundwater level (m below ground surface)	Fluctuation, expressed as the standard deviation around the mean (m)
S0 (Fig. 4a)	**Base scenario** with historical data from reference well 71_1	**0.75**; observation data (Fig. 3)	**0.39**; observation data (Fig. 3)
S0 (not illustrated)*	*Same mean GWL as in scenario S0, all fluctuations removed*	*0.75; observation data (Fig. 3)*	*0; no fluctuations (time-invariant)*
S1 (Fig. 4b)	**Increased annual average GWL** compared with S0	**0.55**; 0.2 m closer to surface than S0	**0.39**; same as S0
S1 (not illustrated)*	*Same mean GWL as in scenario S1, all fluctuations removed*	*0.55; 0.2 m closer to surface than S0*	*0; no fluctuations (time-invariant)*
S2 (Fig. 4c)	**Increased GWL fluctuations around the mean** compared with S0	**0.75**; same as S0	**0.58**; S1 amplified by 1.5
S3 (Fig. 4d)	**Increased GWL as well as increased fluctuations** compared with S0	**0.55**; 0.2 m closer to surface than S0	**0.58**; S1 amplified by 1.5
S4 (Fig. 4d)	**Increased GWL but decreased fluctuations** compared with S0	**0.55**; 0.2 m closer to surface than S0	**0.26**; S1 reduced by 1/1.5 = 0.67

Bold: Scenarios that account for GWL fluctuations. Italics: Scenarios that neglect GWL fluctuations.
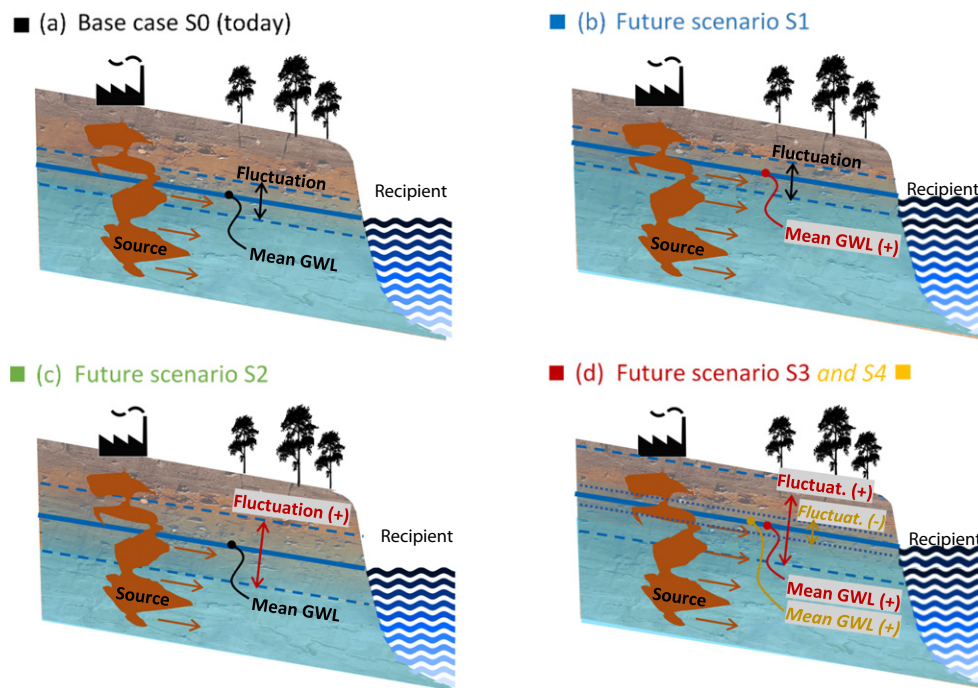
Fig. 4. Schematic illustrations of the mean groundwater level (GWL) and fluctuation around the mean level at a metal-contaminated site, considering (a) current conditions, and possible scenarios for future conditions: (b) increased mean GWL, (c) increased amplitude of GWL fluctuations around the mean level, and (d) combinations involving both increased mean GWL and changed amplitude of GWL fluctuations. The scenarios are summarized in Table 4 and the corresponding GWL input data series are plotted in Fig. 3b and c.

with As(V), since all other conditions were the same (Table 1). The K_d value for As(III) is about 1/20 of the K_d value for As(V), i.e., for a given soil concentration of As in the source zone, the concentration of As(III) partitioned into the aqueous phase will be around 20-fold higher than the As(V) concentration. In addition, the groundwater transport of As (V) will be much more retarded due to the high K_d value of As, which can explain a large part of the multi-fold difference between the As (III) and As(V) mass flows.

The K_d value for Pb was 160-fold higher than that for As(V) in the lower part of the modeled domain (Table 1). The concentration in the aqueous phase was therefore correspondingly lower. Since, for the same reason, Pb is heavily retarded during its transport, the total mass flows of Pb were very low (Fig. 5) in comparison with e.g., the mass flows of As(III) and As(V). On the other hand, the simulation of Pb transport illustrated the general behavior of a fairly immobile element with higher solubility in the upper part of the soil profile. In our example, the higher solubility in the upper 50 cm was due to the transport of Pb with particles that occur in this domain only, which lowered the K_d value by a factor of 11. As a result, the major Pb mass flow occurred in the upper 50 cm in the base scenario (Fig. 5; layers 4 and above), which also made the Pb mass flow strongly responsive to future increases in mean groundwater levels (Fig. 5; scenarios S1, S2, and S3) and changes in the amplitude of groundwater level fluctuations (Fig. 5; scenario S2).

3.3. Consequences of neglecting groundwater level dynamics on projected contaminant loads

Modeled cumulative contaminant mass flows in the whole soil profile in the monitored section (Fig. 1), downstream from the 'source zone', after 41 years (under historical conditions) differed considerably depending on whether or not the model accounted for groundwater level dynamics (Fig. 6). For As(V), which was assumed to have the same K_d value throughout the soil profile, neglecting groundwater level fluctuations (scenario S0* in Fig. 6a) yielded 20% lower cumulative mass flow at the end of the 41-year simulation period compared with

when groundwater level fluctuations were accounted for in S0. For Pb, which was assumed to have a depth-dependent K_d value, the estimated mass loads were completely different when groundwater level fluctuations were neglected (dotted line), and constituted only 0.3% of the end-of-simulation value when the fluctuations were accounted for (solid line), an underestimation of 99.7%.

Similar differences in predicted loads were seen in the modeling results for the future scenarios (Fig. 6b). Neglecting groundwater level fluctuations (S1*) led to systematic underestimation of the future cumulative mass loads for both As and Pb, by some orders of magnitude in the case of Pb. When groundwater level fluctuations were not neglected (S1), the results showed high sensitivity to the assumed magnitude of fluctuations. In the scenario where the fluctuations increase in the future (S3), the estimated cumulative mass flows at the end of the 41-year simulation period were predicted to be about 50% higher for As(V), and 160% higher for Pb, than in the scenario where current observed groundwater level fluctuations remained unchanged in the future (S1).

The systematic errors seen as underpredictions of both current (Fig. 6a) and future (Fig. 6b) mass flows when neglecting groundwater level fluctuations did not disappear when considering relative mass flow changes between current and future conditions (Fig. 6c). In all cases, the differences between future and current conditions were underestimated when groundwater level fluctuations were neglected, by 35–70% in the case of As(V) and by 95–98% in the case of Pb. Even larger differences were seen for the first 5–10 years of the simulation. These derived from contaminant plume evolution and differences in downstream breakthrough between the scenarios, which were much more pronounced at early stages of plume development.

4. Discussion

Our simulations showed that groundwater-borne metal(loid) transport may increase considerably in regions subject to climate-driven increases in mean groundwater level and/or increases in groundwater
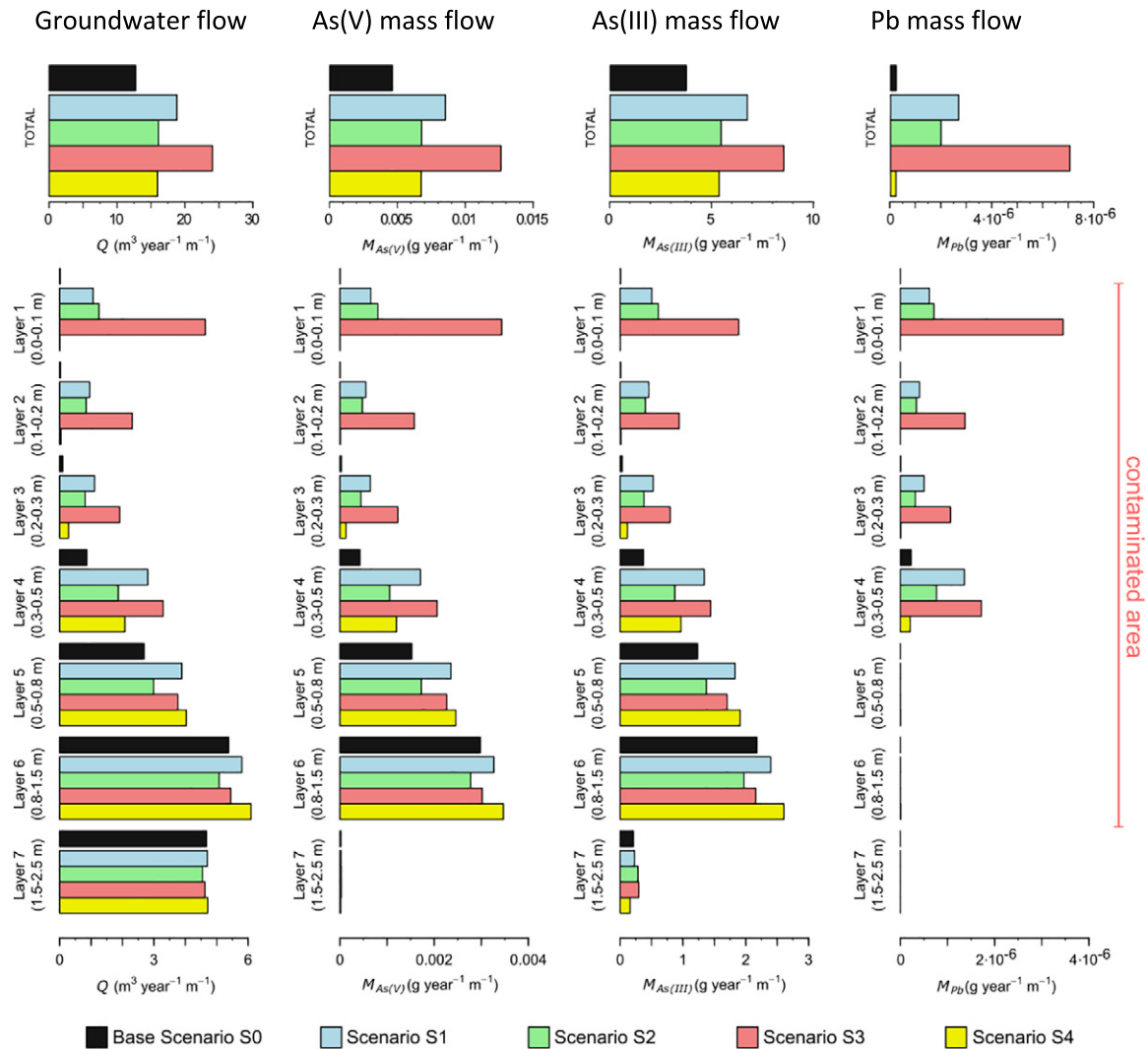
Fig. 5. Total groundwater flow (Q), groundwater flow in each model layer (Q_L) and corresponding mass flows of lead (Pb) (M_{Pb}), arsenate (As(V)) ($M_{As(V)}$), and arsenite (As(III)) ($M_{As(III)}$) just downstream of the contaminated area, given as average values for the 41-year period of historical climate conditions (base scenario, S0, black bars) and average values for four possible future 41-year periods reflecting different climate change scenarios (S1–S4, colored bars).

level variations around the mean. In both cases, the main explanation is that the topsoil will convey a much higher fraction of the total subsurface flow when the groundwater level is shallow, since the hydraulic conductivity of typical northern European and north American till soils increases exponentially with decreasing distance to the soil surface (Mehuys and De Kimpe, 1976; Lind and Lundin, 1990; Nyberg, 1995; Lundmark and Jansson, 2009; Bishop et al., 2011). This finding can be expected to apply also for regions that are not dominated by till soil, as long as the soil is characterized by similar vertical hydraulic conductivity profiles. Considerably elevated saturated hydraulic conductivity in the topsoil has been seen e.g., in peat soils (Boelter, 1968), gley soils (e.g., Musolff et al., 2016), and clay soils (Bathke and Cassel, 1991; McKay et al., 1993). Such conductivity contrasts may also be the result of anthropogenic disturbances, such as an addition of coarse filling material (contaminated) (Wysocka, 2015), which is common in contaminated areas (Löv et al., 2018).

The present study showed that a relatively modest average rise in the groundwater level, of 0.2 m, can evoke total mass flows of As(III) and Pb that are increased by a factor of 1.8 and 12, respectively. This result is consistent with the strong control exerted by groundwater head on element mobilization and export, which is reported for instance regarding nitrate mobilization in a lowland catchment in central

Germany (Musolff et al., 2016), total mercury (Hg) in boreal regions of Sweden (Eklöf et al., 2015), and diffusive cadmium (Cd) and zinc (Zn) emissions in the Netherlands (Bonten et al., 2012).

In general, the simulations showed that the mass flow changes for species with constant K_d values throughout the soil profile, such as As (III) and As(V), were approximately proportional to the water flow changes in the soil. For Pb, the varying geochemical properties along the soil profile (including K_d variations) were the main explanation for the fact that the mass flow of Pb increased more than the groundwater flow. In our example, the total transport of Pb in the more water-conducting topsoil layers was related to facilitated transport of Pb by particles, as also found by Löv et al. (2018) for a contaminated sandy loam. Other factors that can promote higher solubility of metals in upper soil layers compared with deeper layers include higher concentrations of dissolved organic ligands and lower pH values (Gustafsson et al., 2003; Groenenberg et al., 2012). The increase in mass flows of As(III), by a factor of 1000 compared with As(V), illustrate the tremendous impact of going from oxidizing to reducing conditions on mobility of this element. According to Smedley and Kinniburgh (2002), K_d values for As(III) of <0.01 m^3 kg^{-1} have been reported for soils in the USA and groundwater aquifers in Bangladesh, i.e., considerably lower values than applied in the present study.
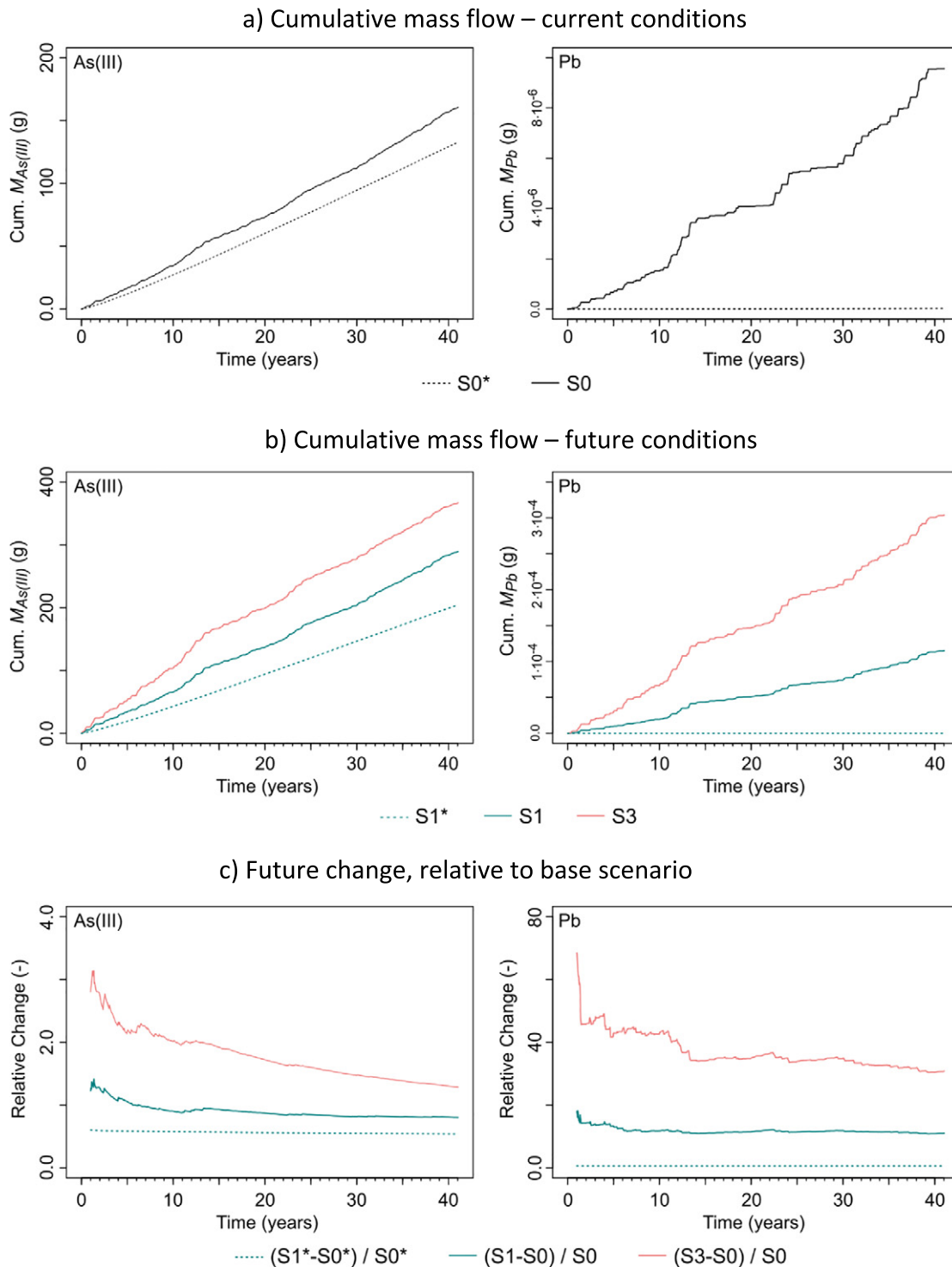
a) Cumulative mass flow – current conditions

b) Cumulative mass flow – future conditions

c) Future change, relative to base scenario

Fig. 6. Modeled cumulative mass flows of arsenate (As(V)) (left column) and lead (Pb) (right column) based on (a) current conditions, using observed long-term average groundwater level (neglecting groundwater level (GWL) fluctuations altogether; dashed line) and using bi-weekly data (accounting for GWL fluctuations; solid line), (b) three future projections that all account for increased GWL, but have different GWL fluctuation assumptions as follows: (i) neglecting GWL fluctuations altogether (blue dashed line), (ii) assuming similar fluctuations in the future as today (S1, blue solid line), and (iii) assuming increased fluctuations in the future (S2, red solid line), and (c) future changes for the same cases as in (b), but expressed as relative change from current conditions by dividing future change scenario results in (b) with base scenario results in (a).

In the context of climate change impacts, increases in heavy metal loads, similar to those presented here for As, have for instance previously been predicted for Zn and Cd in a lowland region of the Netherlands as a result of increased soil leaching and runoff (Wijngaard et al., 2017). The groundwater quality in many regions of

the world may generally be sensitive to such climate-driven hydrological changes, although the governing processes are often complex and difficult to predict (Kløve et al., 2014). Our results show that climate-driven changes in groundwater level alone (without accounting for possible additional changes in leaching) can have large impacts on metal

mobilization. Such groundwater level impacts may be particularly pronounced in downgradient regions, e.g., near surface water recipients, where lateral (regional) groundwater fluxes dominate over (local) vertical fluxes from infiltration and percolation of excess water in the unsaturated zone.

Additional vertical water fluxes and associated downward contaminant fluxes through the unsaturated zone, which were not considered here, may need more attention in future studies. This is particularly true if larger modeling domains are considered (Bonten et al., 2012). Climate-driven increases in effective precipitation (difference between precipitation and evapotranspiration) will arguably exacerbate the impacts of both elevated groundwater levels and increased groundwater flows, and result in additional impacts of increased vertical water fluxes over contaminated areas. This implies that the considerable groundwater level impacts demonstrated in our study may still be underestimates of actual impacts in regions where future effective precipitation will increase.

Our results show that neglecting groundwater level dynamics (e.g., fluctuations around the mean level; here we considered biweekly data) can lead to considerable and systematic underestimation of metal mobilization. In particular, order-of-magnitude differences in predicted cumulative mass flows were seen when geochemical gradients were present in the topsoil, as is the case for Pb, depending on whether or not the model accounted for groundwater level dynamics. Previously, Bonten et al. (2012) presented an example where absolute mass flows were underestimated in models that did not account for dynamic effects. This common conclusion may hence apply for a range of environmental conditions. In addition to the absolute mass flow estimates, we demonstrated for the first time that relative changes (analogous to so-called 'delta changes' in the climate change nomenclature) are considerably underestimated when dynamic effects are neglected. Such effects may arise from intensification of the hydrological cycle and possibly also increased occurrence of extreme weather events (e.g., Olsson and Foster, 2014). Additionally, seasonal changes in precipitation patterns, a shift from precipitation as snow towards precipitation as rain, and earlier snowmelt are expected to impact both groundwater levels and fluctuation amplitudes in Northern Europe (e.g., Vikberg et al., 2015). Therefore, such dynamics, which are not captured by e.g., simple 1D model simulations typically based on the Domenico solution (Domenico, 1987), for example Bioscreen (Newell et al., 1996), need to be considered in future projections for risk assessments and, not least, in the design of risk management strategies.

Quantitative relationships between groundwater level changes and changes in contaminant mobilization, such as those seen in this study and by e.g. Seibert et al. (2009), Bonten et al. (2012), Eklöf et al. (2015) and Musolff et al. (2016), have the potential to reproduce effects of dominant mechanisms and processes, while being simple enough to be applicable to entire catchments or river basins. Although this is a precondition for understanding impacts of hydroclimatic change on large-scale contaminant mobilization, several open questions remain. For instance, although we obtained conclusive results on increased metal(loid) mobilization in regions where groundwater levels or fluctuations will increase the future, it is not clear how such regions can be robustly identified. A main reason is that current models (e.g., coupled climate and hydrological models) appear to be too uncertain to project future changes in groundwater level. This is evidenced by the lack of reported success in reproducing observed, systematic groundwater level changes using (historical) climate model runs. A synthesis by Kløve et al. (2014) showed that the main uncertainties in this regard relate to the predictive understanding of (changes) in spatio-temporal recharge patterns, including potential changes in the mechanisms themselves. This finding is consistent with mounting observational evidence showing that pronounced spatio-temporal differences in groundwater recharge patterns exist in many regions and thus need to be accounted for in predictive models (Jyrkama and Sykes, 2007; Bailey et al., 2016)

Systematic assessments have also shown that the climate models of CMIP5 often fail to reproduce current trends in runoff change in catchments across the northern hemisphere (Bring et al., 2015). Hence, a better quantitative understanding of the related processes is needed to support enhanced region-specific model simulations of hydroclimatic change (Meixner et al., 2016) that can demonstrate the magnitudes and seasonal patterns of future changes in groundwater levels and their fluctuations. The absence of such projections necessitates the use of historical trend analyses to reasonably constrain future scenarios of groundwater level change in scientific assessments, as demonstrated in the present work as well as in previous assessments (Cui et al., 2018; Rodell et al., 2018).

Nevertheless, we note that our future scenarios of groundwater level change, which were constrained by historical groundwater level trends from low-lying groundwater discharge areas, are consistent with more general, large-scale projections of future groundwater level changes. For instance, a synthesis presenting the ensemble result of nine climate model projections of future groundwater level changes in Sweden based on IPCC's Representative Concentration Pathway (RCP) 4.5 trajectory (Vikberg et al., 2015) shows that the whole country except for its south-western part is expected to experience average groundwater level increases of up to 0.2 m, comparing the periods 1961–1990 and 2021–2050. This coincides with our scenario assumption of 0 to 0.2 m. Furthermore, the groundwater level variation around the average value is expected to increase in some parts of Sweden (Vikberg et al., 2015), whereas other parts can expect unchanged or even decreased levels, in consistency with our different scenario assumptions. However, the low spatio-temporal resolution of the results presented in Vikberg et al. (2015) need to be improved to adequately account for the prevailing highly heterogeneous hydrogeological conditions that can have large impact on metal mobilization and transport. If this could be achieved in new model generations - a considerable scientific challenge - their output would directly provide suitable boundary conditions for projecting metal mobilization and transport at individual contaminated sites, using similar groundwater flow simulations as adopted here.

5. Conclusions

- Our simulation results suggest that, in order to understand impacts of climate change on pollutant release from source zones, it is necessary to understand how the contact between groundwater and the highly conductive (and frequently polluted) topsoil layers will change in the future.

- For regions where average groundwater levels are expected to increase in the future, or where the amplitude of groundwater level fluctuations may increase, there is a risk that (metal) contaminants in topsoil will mobilize and spread through the groundwater system to a much larger extent than today. This is particularly true in soil profiles where the hydraulic conductivity increases towards the surface.

- Our results show that neglecting groundwater level dynamics (e.g., fluctuations around the mean) in predictive models can lead to systematic, order-of-magnitude underestimation of metal mobilization and of future relative changes (increases) in metal mobilization. The main reason is that such time-invariant models do not capture the interplay between hydrological and geochemical characteristics in horizontally layered soil profiles.

- For arsenic, the major factor determining the magnitude of climate change effects on transport is the indirect effect of groundwater level and fluctuations on the redox potential. Mass flows of As(III) were shown to be approximately 1000-fold higher than mass flows of As(V), although the K_d value for As(III) was only about 1/20 of that for As(V). This illustrates the need for dynamic modeling approaches when predicting climate change effects on contaminant transport.

- For lead, which is the relatively immobile in soil, the climate change effects can be substantial because of high sensitivity to increased

groundwater levels and fluctuations in these. This is due to the assumed facilitated transport of Pb by particles in the highly conductive topsoil. Thus elements for which solubility increases in the upper part of the soil profile are more prone to climate change-induced changes in groundwater level dynamics.

- This study focused on the role of climate-driven changes in groundwater levels and associated changes in (near-horizontal) shallow groundwater flow on transport of metal pollutants. Other factors not quantified here may also need further attention in future studies. These include climate-driven changes in (vertical) infiltration flux through the unsaturated part of the soil profile and the impact of changes in frequency of catastrophic events, such as landslides, in contaminated areas.

Declaration of competing interest

Acknowledgements

References

Abrahim, G.M.S., Parker, R.J., 2008. Assessment of heavy metal enrichment factors and the degree of contamination in marine sediments from Tamaki Estuary, Auckland, New Zealand. Environ. Monit. Assess. 136, 227–238.

Andersson, I., Jarsjö, J., Petersson, M., 2014. Saving the Baltic Sea, the inland waters of its drainage basin, or both? Spatial perspectives on reducing P-loads in eastern Sweden. Ambio 43 (7), 914–925.

Andersson-Sköld, Y., Nyberg, H., Göransson, G., Lindström, Å., Nordbäck, J., Gustafsson, M., 2007. Föroreningsspridning vid översvämningar och kraftiga flöden -Underlag för Klimat- och sårbarhetsutredningen SOU 2007:60 (In Swedish). Report series SGI Varia 5771100-6692The Swedish Geotechnical Institute, Linköping, Sweden.

Augustsson, A., Philipsson, M., Öberg, T., Bergbäck, B., 2011. Climate change—an uncertainty factor in risk analysis of contaminated land. Sci. Total Environ. 409 (22), 4693–4700.

Bailey, R.T., Wible, T.C., Arabi, M., Records, R.M., Ditty, J., 2016. Assessing regional-scale spatio-temporal patterns of groundwater–surface water interactions using a coupled SWAT-MODFLOW model. Hydrol. Process. 30 (23), 4420–4433.

Barros, C.B., et al., 2014. Technical summary. Climate Change 2014: Impacts, Adaptation and Vulnerability. Part A: Global and Sectoral Aspects. Contribution of Working Group II to the Fifth Assessment Report on the Intergovernmental Panel on Climate Change. Cambridge University Press, Cambridge, United Kingdom and New York, NY; USA.

Barth, J.A.C., Grathwohl, P., Fowler, H.J., Bellin, A., Gerzabek, M.H., Lair, G.J., et al., 2009. Mobility, turnover and storage of pollutants in soils, sediments and waters: achievements and results of the EU project AquaTerra-A review. Agron. Sustain. Dev. 29, 61–173.

Bathke, G.R., Cassel, D.K., 1991. Anisotropic variation of profile characteristics and saturated hydraulic conductivity in an Ultisol landscape. Soil Sci. Soc. Am. J. 55 (2), 333–339.

Bergvall, M., Grip, H., Sjöström, J., Laudon, H., 2011. Modeling subsurface transport in extensive glaciofluvial and littoral sediments to remediate a municipal drinking water aquifer. Hydrol. Earth Syst. Sci. 15 (7), 2229–2244.

Bishop, K., Seibert, J., Nyberg, L., Rodhe, A., 2011. Water storage in a till catchment. II: implications of transmissivity feedback for flow paths and turnover times. Hydrol. Process. 25 (25), 3950–3959.

Boelter, D.H., 1968. Important physical properties of peat material. Proceedings of the Third International Peat Congress. National Research Council of Canada, Quebec City, pp. 150–156.

Bonten, L.T., Kroes, J.G., Groenendijk, P., van der Grift, B., 2012. Modeling diffusive Cd and Zn contaminant emissions from soils to surface waters. J. Contam. Hydrol. 138, 113–122.

Brandon, E., 2013. The nature and extent of site contamination. Global Approaches to Site Contamination Law. Springer, Dordrecht, pp. 11–39. https://doi.org/10.1007/978-94-007-5745-5_2.

Bring, A., Asokan, S.M., Jaramillo, F., Jarsjö, J., Levi, L., Pietroń, J., Prieto, C., Rogberg, P., Destouni, G., 2015. Implications of freshwater flux data from the CMIP5 multimodel output across a set of Northern Hemisphere drainage basins. Earth's Future 3. https://doi.org/10.1002/2014EF000296.

Clark, M.P., Fan, Y., Lawrence, D.M., Adam, J.C., Bolster, D., Gochis, D.J., Hooper, R.P., Kumar, M., Leung, L.R., Mackay, D.S., Maxwell, R.M., Shen, C., Swenson, S.C., Zeng, X., 2015. Improving the representation of hydrologic processes in Earth System Models. Water Resour. Res. 51 (8), 5929–5956.

Colombani, N., Dinelli, E., Mastrocicco, M., 2016. Trend of heavy metal release according to forecasted climate change in the Po Delta. Environmental processes 3 (3), 553–567.

Cui, T., Raiber, M., Pagendam, D., Gilfedder, M., Rassam, D., 2018. Response of groundwater level and surface-water/groundwater interaction to climate variability: Clarence-Moreton Basin, Australia. Hydrogeol. J. 26 (2), 593–614.

Destouni, G., Persson, K., Prieto, C., Jarsjö, J., 2010. General quantification of catchment-scale nutrient and pollutant transport through the subsurface to surface and coastal waters. Environmental Science & Technology 44 (6), 2048–2055.

Domenico, P.A., 1987. An analytical model for multidimensional transport of a decaying contaminant species. J. Hydrol. 91, 49–58.

Eckhardt, K., Ulbrich, U., 2003. Potential impacts of climate change on groundwater recharge and streamflow in a central European low mountain range. J. Hydrol. 284 (1–4), 244–252.

Eklöf, K., Kraus, A., Futter, M., Schelker, J., Meili, M., Boyer, E.W., Bishop, K., 2015. Parsimonious model for simulating total mercury and methylmercury in boreal streams based on riparian flow paths and seasonality. Environmental Science & Technology 49 (13), 7851–7859.

Fanger, G., Elert, M., Höglund, L.O., Jones, C., 2006. Laktester för riskbedömning av förorenade områden – Underlagsrapport 3: Sammanställning av underlagsdata och användning av modeller för tolkning av laktester. Swedish EPA (Report no 5558).

Groenenberg, J.E., Dijkstra, J.J., Bonten, L.T.C., de Vries, W., Comans, R.N.J., 2012. Evaluation of the performance and limitations of empirical partition-relations and process based multisurface models to predict trace element solubility in soils. Environ. Pollut. 166, 98–107.

Gustafsson, J.P., Pechová, P., Berggren, D., 2003. Modeling metal binding to soils: the role of natural organic matter. Environmental Science & Technology 37, 2767–2774.

Hashim, M.A., Mukhopadhyay, S., Narayan Sahu, J., Senguptab, B., 2011. Remediation technologies for heavy metal contaminated groundwater. J. Environ. Manag. 92 (10), 2355–2388.

IPCC, 2014. Summary for policymakers. Climate Change 2014: Impacts, Adaptation, and Vulnerability. Part A: Global and Sectoral Aspects. Contribution of Working Group II to the Fifth Assessment Report of the Intergovernmental Panel on Climate Change. Cambridge University Press, Cambridge, United Kingdom and New York, NY; USA.

Jaishankar, M., Tseten, T., Anbalagan, N., Mathew, B.B., Beeregowda, K.N., 2014. Toxicity, mechanism and health effects of some heavy metals. Interdisciplinary Toxicology 7 (2), 60–72.

Jarsjö, J., Chalov, S.R., Pietroń, J., Alekseenko, A.V., Thorslund, J., 2017a. Patterns of soil contamination, erosion and river loading of metals in a gold mining region of Northern Mongolia. Reg. Environ. Chang. 17, 1991–2005.

Jarsjö, J., Törnqvist, R., Su, Y., 2017b. Climate-driven change of nitrogen retention – attenuation near irrigated fields: multi-model projections for Central Asia. Environ. Earth Sci. 76, 117.

Jyrkama, M.I., Sykes, J.F., 2007. The impact of climate change on spatially varying groundwater recharge in the grand river watershed (Ontario). J. Hydrol. 338 (3–4), 237–250.

Karthe, D., Abdullaev, I., Boldgiv, B., Borchardt, D., Chalov, S., Jarsjö, J., Li, L., Nittrouer, J.A., 2017. Water in Central Asia: an integrated assessment for science-based management. Environ. Earth Sci. 76, 690.

Kløve, B., Ala-Aho, P., Bertrand, G., Gurdak, J.J., Kupfersberger, H., Kværner, J., Muotka, T., Mykrä, H., Preda, E., Rossi, P., Uvo, C.B., 2014. Climate change impacts on groundwater and dependent ecosystems. J. Hydrol. 518, 250–266.

Lidman, F., Boily, Å., Laudon, H., Köhler, S.J., 2017. From soil water to surface water–how the riparian zone controls element transport from a boreal forest to a stream. Biogeosciences 14 (12), 3001–3014.

van Liedekerke, M., Prokop, G., Rabl-Berger, S., Kibblewhite, M., Louwagie, G., 2014. Progress in the Management of Contaminated Sites in Europe, European Commission EUR 26376. EUR – Scientific and Technical Research SeriesPublications Office of the European Union, Luxembourg (ISSN 1831-9424 (online), ISBN 978-92-79-34846-4 (PDF), doi:10.2788/4658, doi:10.2788/4658).

Lind, B.B., Lundin, L., 1990. Saturated hydraulic conductivity of Scandinavian tills. Hydrol. Res. 21 (2), 107–118.

Löv, Å., Cornelis, G., Larsbo, M., Sjöstedt, C., Persson, I., Gustafsson, J.P., Boye, K., Kleja, D.B., 2018. Particle and colloid facilitated Pb leaching in four historically contaminated soils – speciation and effect of irrigation intensity. Appl. Geochem. 96, 327–338.

Lundin, L., 1982. Soil moisture and ground water in till soil and the significance of soil type for runoff. Ph.D. dissertation. UNGI Report No. 56. Uppsala University, p. 216 (in Swedish).

Lundmark, A., Jansson, P.E., 2009. Generic soil descriptions for modelling water and chloride dynamics in the unsaturated zone based on Swedish soils. Geoderma 150 (1), 85–95.

McKay, L.D., Cherry, J.A., Gillham, R.W., 1993. Field experiments in a fractured clay till: 1. Hydraulic conductivity and fracture aperture. Water Resour. Res. 29 (4), 1149–1162.

Mehuys, G.R., De Kimpe, C.R., 1976. Saturated hydraulic conductivity in pedogenetic characterization of podzols with fragipans in Quebec. Geoderma 15 (5), 371–380.

Meixner, T., Manning, A.H., Stonestrom, D.A., Allen, D.M., Ajami, H., Blasch, K.W., et al., 2016. Implications of projected climate change for groundwater recharge in the western United States. J. Hydrol. 534, 124–138.

Mulligan, C.N., Yong, R.N., Gibbs, B.F., 2001. Remediation technologies for metal-contaminated soils and groundwater evaluation. Eng. Geol. 60, 193–207.

Musolff, A., Schmidt, C., Rode, M., Lischeid, G., Weise, S.M., Fleckenstein, J.H., 2016. Groundwater head controls nitrate export from an agricultural lowland catchment. Adv. Water Resour. 96, 95–107.

Nagajyoti, P.C., Lee, K.D., Sreekanth, T.V.M., 2010. Heavy metals, occurrence and toxicity for plants: a review. Environ. Chem. Lett. 8 (3), 199–216.

Naser, H.A., 2013. Assessment and management of heavy metal pollution in the marine environment of the Arabian Gulf: a review. Mar. Pollut. Bull. 72 (1), 6–13.

Newell, C.J., McLeod, R.K., Gonzales, J.R., 1996. Bioscreen: Natural Attenuation Decision Support System. User's Manual Version 1.3. U.S. EPA Office of Research and Development, Washington DC.

Newton, A., Carruthers, T.J.B., Icely, J., 2012. The coastal syndromes and hotspots on the coast. Estuar. Coast. Shelf Sci. 96, 39–47.

Nyberg, L., 1995. Water flow path interactions with soil hydraulic properties in till soil at Gårdsjön, Sweden. J. Hydrol. 170 (1–4), 255–275.

Okkonen, J., Kløve, B., 2011. A sequential modelling approach to assess groundwater–surface water resources in a snow dominated region of Finland. J. Hydrol. 411 (1–2), 91–107.

Olsson, J., Foster, K., 2014. Short-term precipitation extremes in regional climate simulations for Sweden. Hydrol. Res. 45 (3), 479–489.

Pédrot, M., Dia, A., Davranche, M., Bouhnik-Le Coz, M., Henin, O., Gruau, G., 2008. Insights into colloid-mediated trace element release at the soil/water interface. Journal of Colloid Interface Science 325, 187–197.

Persson, K., Jarsjö, J., Destouni, G., 2011. Diffuse hydrological mass transport through catchments: scenario analysis of coupled physical and biogeochemical uncertainty effects. Hydrol. Earth Syst. Sci. 15, 3195–3206.

Pietroń, J., Nittrouer, J.A., Chalov, S.R., Dong, T.Y., Kasimov, N., Shinkareva, G., Jarsjö, J., 2018. Sedimentation patterns in the Selenga River delta under changing hydroclimatic conditions. Hydrol. Process. 32, 278–292.

Raguž, V., Jarsjö, J., Grolander, S., Lindborg, R., Avila, R., 2013. Plant uptake of elements in soil and pore water: field observations versus model assumptions. J. Environ. Manag. 126, 147–156.

Rodell, M., Famiglietti, J.S., Wiese, D.N., Reager, J.T., Beaudoing, H.K., Landerer, F.W., Lo, M.H., 2018. Emerging trends in global freshwater availability. Nature 557 (7707), 651.

Rodhe, A., Lindström, G., Dahné, J., 2009. Grundvattennivåer i ett förändrat klimat. Final report from the Swedish Geological Survey (SGU) Project no 60–1642/2007 44 pp (in Swedish).

Schiedek, D., Sundelin, B., Readman, J.-W., Macdonald, R.W., 2007. Interactions between climate change and contaminants. Mar. Pollut. Bull. 54 (12), 1845–1856.

Scott, J., Beydoun, D., Amal, R., Low, G., Cattle, J., 2005. Landfill management, leachate generation, and leach testing of solid wastes in Australia and overseas. Crit. Rev. Environ. Sci. Technol. 35 (3), 239–332.

Seibert, J., Grabs, T., Köhler, S., Laudon, H., Winterdahl, M., Bishop, K., 2009. Linking soil- and stream-water chemistry based on a Riparian flow-concentration integration model. Hydrol. Earth Syst. Sci. 13 (12), 2287–2297.

SGU, 2017. Sveriges geologiska undersökning. Groundwater levels. [Online]. https://apps.sgu.se/kartvisare/kartvisare-grundvattenniva.html, Accessed date: 1 November 2017.

Smedley, P.L., Kinniburgh, D.G., 2002. A review of the source, behaviour and distribution of arsenic in natural waters. Appl. Geochem. 17, 517–568.

Ströberg, A., Ebert, K., Jarsjö, J., Frampton, A., 2017. Contaminated area instability along Ångermanälven River, Northern Sweden. Environ. Monit. Assess. 189, 118.

Su, Y., Langhammer, J., Jarsjö, J., 2017. Geochemical responses of forested catchments to bark beetle infestation: evidence from high frequency in-stream electrical conductivity monitoring. J. Hydrol. 550, 635–649.

Sundén, G., Maxe, L., Dahné, J., 2010. Grundvattennivåer och vattenförsörjning vid ett förändrat klimat. Swedish Geological Survey (SGU) Report no 2010:12 44 pp (in Swedish).

Sutinen, R., Hänninen, P., Venäläinen, A., 2007. Effect of mild winter events on soil water content beneath snowpack. Cold Reg. Sci. Technol. 51 (1), 56–67.

Swedish EPA, 2017. Description of the management of contaminated sites 2016 (in Swedish, Lägesbeskrivning av arbetet med efterbehandling av förorenade områden 2016, Ärende nummer NV 03165–16, Skrivelse till regeringen 2017-04-06), Letter to the Government 2017-04-06, Case number NV-03165-16. Swedish Environmental Protection Agency http://www.naturvardsverket.se/upload/sa-mar-miljon/mark/fororenade-omraden/lagesbeskrivning-2016-ebh-objekt.pdf (180212).

Thorslund, J., Jarsjö, J., Jaramillo, F., Jawitz, J.W., Manzoni, S., Basu, N.B., et al., 2017. Wetlands as large-scale nature-based solutions: status and challenges for research, engineering and management. Ecol. Eng. 108, 489–497.

Törnqvist, R., Jarsjö, J., Karimov, B., 2011. Health risks from large-scale water pollution: trends in Central Asia. Environ. Int. 37, 435–442.

Tóth, G., Hermann, T., Da Silva, M.R., Montanarella, L., 2016. Heavy metals in agricultural soils of the European Union with implications for food safety. Environ. Int. 88, 299–309.

Vikberg, E., Thunholm, B., Thorsbrink, M., Dahné, J., 2015. Grundvattennivåer i ett förändrat klimat–nya klimatscenarier. Swedish Geological Survey (SGU) Report no 2015:19 26 pp (in Swedish).

Wijngaard, R.R., van der Perk, M., van der Grift, B., de Nijs, T.C.M., Bierkens, M.F.P., 2017. The impact of climate change on metal transport in a lowland catchment. Water Air and Soil Pollution 228 (3), 107.

Wilkie, J.A., Hering, J.G., 1996. Adsorption of arsenic onto hydrous ferric oxide: effects of adsorbate/adsorbents ratios and co-occurring solutes. Colloids and Surfaces A: Physicochemical Engineering Aspects 107, 97–110.

WorldClim, 2018. WorldClim Gloval Climate Data – Free climate data for ecological modelling. [Online]. http://www.worldclim.org/cmip5_2.5m, Accessed date: 1 March 2018.

Wysocka, M.E., 2015. Influence of location of landfills on groundwater quality. Rocznik Ochrona Środowiska 17 (cz. 2), 1074–1093.